Materials Advances

ROYAL SOCIETY OF CHEMISTRY

PAPER

View Article Online
View Journal

Cite this: DOI: 10.1039/d5ma01506e

Oxidation of sp- and sp^2-hybridised molecular semiconductors with iron(III) chloride in organic media

Elda Sala,[ab] João Paulo V. Damasceno,*[c] Stefano Pecorario,[d] Pietro Marabotti,[e] Ivan K. Ilic,[a] Valerio Galli,[af] Simone Melesi,[b] Pierfrancesco Sansò,[ab] Andrea Tuarivoli,[ab] Carlo S. Casari,[b] Daniele Fazzi,[g] Rik R. Tykwinski[h] and Mario Caironi*[a]

Access to the charged states of emerging organic molecular semiconductors is crucial to understand their electronic properties. In the case of materials optimised for hole transport, oxidation can be challenging for molecules with deep HOMO levels. Beyond some of the more common sp^2-molecules, such as acenes and nanographenes, molecules based on sp-hybridised carbon, namely cumulenes, are emerging as materials with unique electronic properties, and good hole transport in field-effect devices based on polycrystalline thin-films. Very little is known, however, about the nature of the charged states contributing to charge transport in cumulenes. In this study, we demonstrate a successful chemical oxidation strategy of two model systems using sp- and sp^2-hybridised molecular semiconductors with deep HOMO levels using iron(III) chloride in optimised organic solvent mixtures. The optimisation process relies on controlling the solvent environment. In the case of the model cumulene tetraphenylbutatriene ([3]Ph), the formation of the oxidised species [3]Ph$^+$ exploits the sp-carbon backbone to accommodate the excess positive charge, and the charge delocalisation dramatically increases the bond length alternation leading to a polyynic structure. We extend this approach to the sp^2 semiconductor C8-BTBT, validating its general applicability. Our findings offer insights into the redox behavior of sp-carbon systems and provide a robust chemical route to access charged states in sp- and sp^2-hybridised small molecules.

Received 23rd December 2025,
Accepted 10th February 2026

DOI: 10.1039/d5ma01506e

rsc.li/materials-advances

Introduction

The interest in organic electronics and emerging optoelectronic and bioelectronic applications has driven the investigation of organic semiconductors, aiming to discover new materials and enhance the performance of existing ones. Conjugated small molecules are typically the best-performing structures among organic semiconductors when employed in field-effect transistors due to their ability to form highly crystalline films.[1,2] Recently, cumulenic carbon atom wires, also referred to as [*n*]cumulenes, have been introduced as an intriguing class of conjugated organic molecules and have offered a new paradigm for organic electronics.[3] Unlike the majority of conjugated organic materials, which rely on sp^2-hybridised carbon, cumulenes are based on sp-hybridisation, and they feature a contiguous series of quasi-double bonds as their backbone.[4–10]

Like polyynes, which are sp-carbon systems constructed from a chain of alternating single and triple bonds,[4–6] cumulenes can be considered finite segments of the elusive sp-carbon allotrope, carbyne.[4,10–12] Carbyne is the ideal, infinitely long carbon chain with one-atom cross section, a truly 1D system,[4,6,10,11] with impressive predicted materials performance,[3,4,10] including a Young modulus as high as 32 TPa[13] and thermal conductivity between 80 and 200 kW m^{-1} K^{-1}.[14] From an electronic point of view, carbyne has two degenerate and orthogonal π-systems with no fixed nodal plane that spans along the entire carbon wire and affords extended charge delocalisation.[4,5,7,10,15–21] Yet, long sp-hybridised carbon chains are highly reactive, and as a consequence, carbyne systems have not yet been isolated.[4,5,7,10–12,22] To date, only finite-length isolated sp-carbon chains, cumulenes and

[a] *Center for Nano Science and Technology, Istituto Italiano di Tecnologia, Milan 20134, Italy. E-mail: mario.caironi@iit.it*
[b] *Department of Energy, Politecnico di Milano, Milan 20156, Italy*
[c] *Department of Inorganic Chemistry, Institute of Chemistry (IQ), University of Campinas (UNICAMP), Campinas (13083-970), Brazil*
[d] *Cavendish Laboratory, University of Cambridge, Cambridge CB3 0HE, UK*
[e] *Institut für Physik, Humboldt Universität zu Berlin, Berlin (12489), Germany*
[f] *Department of Physics, Politecnico di Milano, Milan 20133, Italy*
[g] *Dipartimento di Chimica "Giacomo Ciamician", Università di Bologna, Bologna 40129, Italy*
[h] *Department of Chemistry, University of Alberta, Edmonton T6G 2G2, Alberta, Canada*

polyynes, could be synthesised, thanks to the increased stability, typically favored by bulky end-groups. Such terminations shield the molecule backbone with their steric hindrance, effectively protecting the reactive sp-hybridized framework.[4,7,9–12] Through appropriate selection of the end-groups, in combination with the modulation of the sp-carbon chain length, it is possible to regulate the energy gap and, generally, the electronic energy levels of the molecule, allowing a high degree of electronic tunability.[4,5,7,9,10,23–25] On the one hand, studies on these finite molecules can provide knowledge that may be useful in the effort to isolate the ideal allotrope.[5,10,11] On the other hand, they offer a novel set of versatile conjugated molecules and 1-D nanostructures with tunable optoelectronic properties that can be exploited for organic electronics.

Aside from single-molecule junctions,[26–28] polyynic segments have been tested in white organic light emitting diodes.[29] Meanwhile, cumulenes, especially tetraphenylbutatriene ([3]Ph), are being employed in devices such as supercapacitors[30] and organic field effect transistors (OFETs).[3,31] Notably, [3]Ph-based OFETs exhibited a hole field effect mobility of 0.2 $cm^2 V^{-1} s^{-1}$, as well as ideal transfer characteristics and mobility behavior, and good operational stability.[3] Such promising performance in solid-state devices is not yet fully understood in terms of charge transport mechanisms and the nature of the charged states involved in the transfer processes. To fully exploit the potential of these materials, it is crucial to understand how charges behave when (de)localised around the sp-carbon-based molecules. Accessing the charged states by chemical means is a common approach to studying organic semiconductors, but the oxidation of organic small molecules such as cumulenes can be challenging under typical experimental conditions. Their HOMO (highest occupied molecular orbital) energy level is typically below −5.4 V,[3,32] deeper with respect to common molecular p-dopants. An energy level mismatch between the semiconducting molecule and the oxidant can hinder charge transfer,[33] so a strategy to increase oxidation efficiency is needed.

In this study, we achieve chemical oxidation of cumulene [3]Ph (Fig. 1(a)). To be able to isolate the single molecules, we opted to work on solutions, and detail the conditions that enable this oxidative process, through a combination of

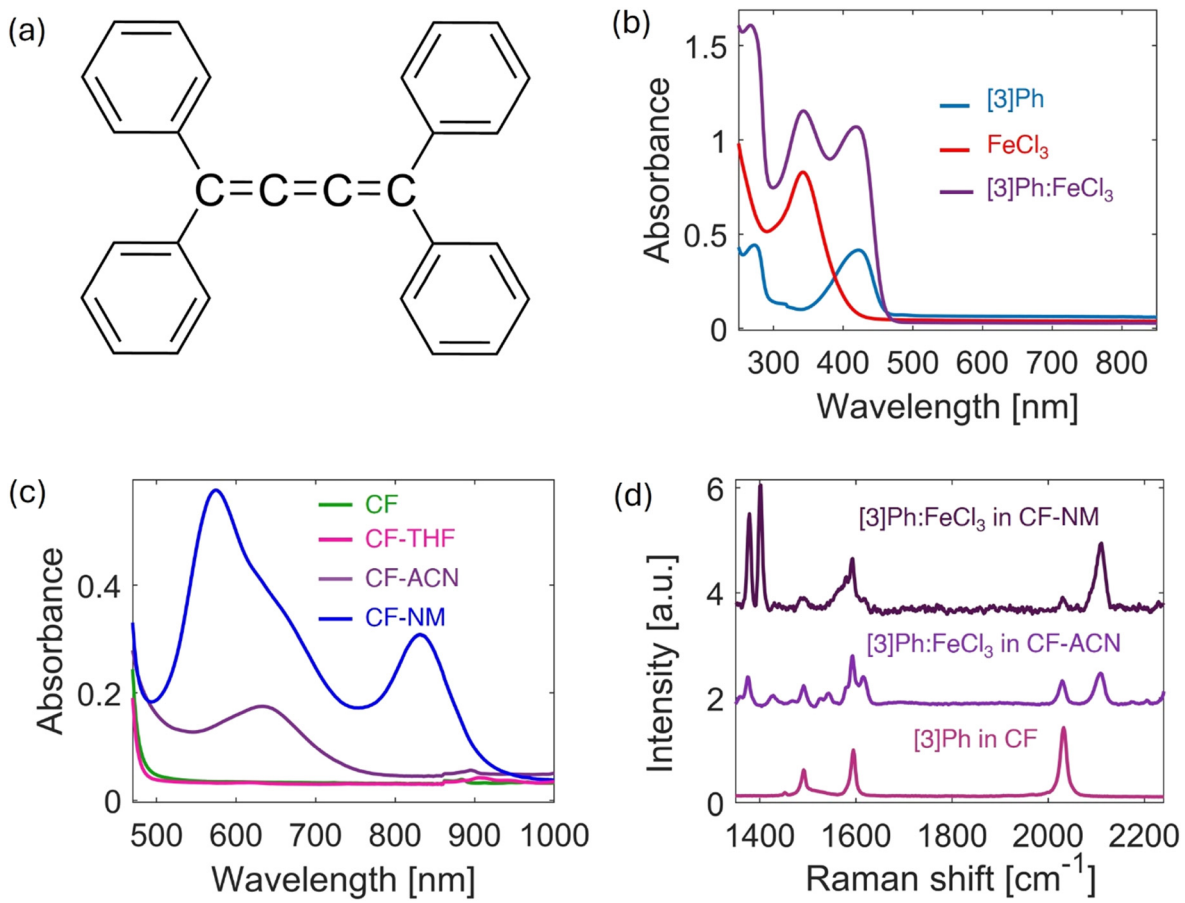

Fig. 1 (a) Molecular structure of the cumulene tetraphenylbutatriene, [3]Ph. (b) UV-Vis-NIR spectra of [3]Ph (0.01 g L^{-1}), $FeCl_3$ (0.05 g L^{-1}), and of [3]Ph and $FeCl_3$ (0.025 g L^{-1}/0.075 g L^{-1}, respectively) in chloroform (CF). (c) UV-Vis-NIR spectra of mixtures of [3]Ph and $FeCl_3$ (0.25 g L^{-1} and 0.75 g L^{-1}, respectively) in CF, CF and tetrahydrofuran (CF–THF), CF and acetonitrile (CF–ACN), and CF and nitromethane (CF–NM), all solvents 1 : 1 volume ratio. A 4 mm optical-path, quartz cuvette was employed to record these spectra. The abrupt step at 860 nm is due to a detector change. (d) Raman spectra of pristine [3]Ph (0.75 g L^{-1}) in CF; [3]Ph and $FeCl_3$ (0.75 g L^{-1}/2.25 g L^{-1}, respectively) in CF–ACN; and [3]Ph and $FeCl_3$ (0.25 g L^{-1}/0.75 g L^{-1}, respectively) in CF–NM. Solvents are mixed in a 1 : 1 volume ratio. Raman intensities are normalised to the peaks around 1600 cm^{-1} for each curve.

spectroscopic, electrochemical, and quantum-chemical techniques. In particular, we describe how the careful choice of the solvent and concentration leads to optimisation of the oxidising mixture to achieve effective oxidation of [3]Ph using $FeCl_3$. Importantly, Raman spectroscopy provides evidence that the charge formed on [3]Ph is hosted by the sp-carbon backbone, a critical step to further understand charge transport properties in this class of materials. Finally, this new oxidation approach is extended to an sp^2-conjugated molecular semiconductor, dioctyl[1]benzothieno[3,2-*b*][1]benzothiophene (known as C8-BTBT), toward establishing a useful and broad strategy for chemical oxidation of conjugated molecules with deep lying HOMO energy levels.

Results and discussion

Since the HOMO level of [3]Ph has been estimated at −5.48 eV,[3] $FeCl_3$ was employed as an oxidant, since in its anhydrous form[34] it is established as a strong and efficient electron acceptor for the oxidation of organic semiconductors.[33,35–42] Chloroform (CF) was the starting solvent of choice, as it is a very good solvent for [3]Ph and there is extensive literature regarding organic molecules oxidised by $FeCl_3$ in chloroform.[34,37,38,40,42–44] The UV-vis-NIR absorption spectra of chloroform solutions of [3]Ph (0.01 g L^{-1}), $FeCl_3$ (0.05 g L^{-1}), and a mixture of [3]Ph and $FeCl_3$ (0.025 g L^{-1} and 0.075 g L^{-1}, respectively, 1 : 6.6 molar ratio) are shown in Fig. 1(b). [3]Ph shows an intense absorption peak with a maximum at about 423 nm, referred to its HOMO–LUMO (lowest unoccupied molecular orbital) transition (with contributions from HOMO−1 → LUMO and HOMO → LUMO+1) and another absorption at 274 nm assigned to the HOMO−1 → LUMO+1.[3,5,7] The spectrum of $FeCl_3$ in CF presents a band at 341 nm associated with the solubilised monomeric species. This value is close to that reported in the literature (336 nm)[44] and attributed to a ligand-to-metal charge transfer excitation. Neither $FeCl_3$ nor [3]Ph has absorption bands above 500 nm. The mixture of [3]Ph and $FeCl_3$ (0.025 g L^{-1} and 0.075 g L^{-1}, respectively) shows absorption features that are best described as a linear combination of the two pristine compounds, leading to the conclusion that a reaction between [3]Ph and the oxidant $FeCl_3$ has not occurred.

To force oxidation, the concentration of both [3]Ph and $FeCl_3$ was increased. Fig. S1 shows the UV-vis-NIR absorption spectra of the mixtures of the two reagents in CF at different concentrations, keeping the molar ratio of [3]Ph : $FeCl_3$ fixed at 1 : 6.6, with an excess of oxidant. Concentration values up to 0.5 g L^{-1}/1.5 g L^{-1} ([3]Ph/$FeCl_3$) did not produce new optical features. A mixture at 1 g L^{-1}/3 g L^{-1} displayed weak new bands at 573, 615, 697, and 786 nm, partially covered by scattering, consistent with the formation of an oxidised product, as neither the cumulene nor the solvent is expected to act as a ligand for iron(III).[45–47] The amount of $FeCl_3$ can be reduced, and the new optical features can be made cleaner if the oxidation of [3]Ph is stabilised by favorable intermolecular interactions, which shifts the equilibrium towards the oxidised product. A more polar solvent provides strong intermolecular interactions, favoring the formation of polar/ionic species both kinetically and thermodynamically.[48] On this basis, the oxidation of [3]Ph (0.25 g L^{-1}) was explored using reduced concentrations of $FeCl_3$ (0.75 g L^{-1}) while adding an aprotic, polar solvent along with CF in a 1 : 1 volume ratio, including acetonitrile (ACN), nitromethane (NM), and tetrahydrofuran (THF). The UV-vis-NIR spectra of these mixtures above 450 nm are presented in Fig. 1(c). In pure CF at this concentration, as expected, there is no change in the spectrum. Likewise, attempted oxidation in the mixture of CF and THF does not present any new features. On the other hand, the system containing ACN shows the emergence of a new band in the visible region, at about 634 nm, indicating a reaction between [3]Ph and $FeCl_3$. The sample containing NM shows two pronounced new bands at 574 and 831 nm, in addition to the feature at 634 nm. This confirms that a reaction, presumed to be the oxidation of [3]Ph, took place. Time-dependent density functional theory (TD-DFT) calculations (ωB97X-D/cc-pVTZ level of theory, see Fig. S2 and S3) performed on the mono-oxidised product [3]Ph^+, compute the first dipole-allowed transition at 1.94 eV (638.6 nm, unscaled energy value), with an oscillator strength (*f*) of 0.253. The character of such D_0–D_1 transition (*i.e.*, ground to first excited state transition of positively charged, Doublet, species, D) is represented by a SOMOα to SUMOα excitation (Single (Un)Occupied Molecular Orbitals), thus involving the frontier π–π* MOs of the oxidised species and showing electron density contributions from both the carbon chain atoms and the aryl groups (Fig. S2). Due to the well-known overestimation of the transition energies as computed with the range-separated DFT functional,[49,50] we can safely assign this transition to that observed experimentally at around 831 nm. The computed spectrum of the oxidised species also shows two additional transitions, centered at around 500 nm (see Fig. S2), which are red shifted with respect to the absorption of the neutral species (computed at 384 nm, f = 0.93). These transitions can be assigned to the experimental absorption bands at around 600 nm (Fig. 1(c), CF–NM spectrum).

Beyond UV-vis spectroscopic analysis, the oxidation of [3]Ph to [3]Ph^+ was also corroborated by the Raman spectra (Fig. 1(d)), as Raman is an unambiguous technique to detect sp-carbon species.[9,23,51,52] The Raman spectrum of pure [3]Ph (0.75 g L^{-1} in CF) shows a peak at 2030 cm^{-1} in the spectral region of the characteristic vibration of cumulenes and other sp-carbon-based materials (*i.e.*, from 1800 to 2200 cm^{-1}).[4,9,23,24,53–55] This vibration is assigned to the so-called ECC mode, from the effective conjugation coordinate theory,[4,23] and refers to a collective in-phase stretching and shrinking of the sp-carbon bonds. The Raman spectrum of the mixture of [3]Ph and $FeCl_3$ (0.75 g L^{-1} and 2.25 g L^{-1}, respectively; the concentrations were increased with respect to UV-vis absorption measurements to ensure a strong Raman signal) in CF–ACN (1 : 1 volume ratio) exhibits an additional blue-shifted peak centered at 2100 cm^{-1}, consistent with the oxidation of [3]Ph to [3]Ph^+. A comparison of the DFT computed Raman spectra of [3]Ph and [3]Ph^+ (see Fig. S2) shows a blue shift of the ECC Raman active mode upon oxidation, from 2202 cm^{-1} to 2235 cm^{-1}, respectively

(ωB97X-D/cc-pVTZ, unscaled value). The blue shift is correlated to an increase in the bond length alternation (BLA) of the sp carbon–carbon bonds, from 0.07 Å to 0.14 Å, upon oxidation (Fig. S3), *i.e.*, increased polyynic-like character of the chain in the charged state.[4,5,7,9,23,56] The combined experimental and computational Raman results support the formation of a sp-carbon system for the oxidised species, as this vibrational mode still falls into the ECC mode region. As further proof, Raman spectra were acquired for a mixture of $FeCl_3$ in CF–ACN, and in CF–NM (1 : 1 by volume), neither of which displays a signal in the sp-carbon region (Fig. S4). Thus, we conclude that [3]Ph is oxidised by $FeCl_3$ to give [3]Ph$^+$, which features a structure with the positive charge localised mainly on the sp-carbon backbone.[55] In the case of [3]Ph and $FeCl_3$ (0.25 g L^{-1} and 0.75 g L^{-1}, respectively) in CF–NM (1 : 1 by volume), the new feature at 2100 cm^{-1} is much more pronounced compared to that of [3]Ph at 2030 cm^{-1}, despite the lower concentrations used, consistent with an increased oxidation efficiency promoted by NM, as observed in the UV-vis-NIR spectra (Fig. 1(c)).

The oxidation of [3]Ph by $FeCl_3$ is further supported by the Raman peaks between 1500 and 1650 cm^{-1}. When oxidised, the symmetric aryl stretching modes of neutral [3]Ph at 1596 cm^{-1} split into two Raman active modes at 1581 and 1614 cm^{-1}, respectively (Fig. 1(d)). Such normal modes represent a quinoidal-like oscillation of the aryl units, with frequencies red-shifted with respect to the neutral species. Such observation is supported by DFT calculations (see Fig. S2 and S3), which reveal slight variations in the aryl carbon–carbon bond-lengths and dihedral angles upon oxidation, thus leading to a change in the force constants that justifies the frequency red-shift. Interestingly, the low-frequency peak does not present particular solvent-dependent intensity modulation, the high-frequency one presents a remarkable intensity in CF–ACN compared to the CF–NM solution. These observations point toward the assignment of the peak at 1614 cm^{-1} to Fe^{3+}-mediated complexes with the aryl rings of [3]Ph. Indeed, given the lower oxidation efficiency of [3]Ph in CF–ACN, a greater fraction of [3]Ph might be engaged in $FeCl_3$–ACN coordination complexes than in direct $FeCl_3$-[3]Ph ones, resulting in a higher intensity of the high-frequency Raman peak compared to CF–NM solution (*vide infra*). Regarding the other Raman signals observed in the spectra in Fig. 1(d), the peak at about 1492 cm^{-1} in [3]Ph, related to a combined vibration of C=C, C–C, and C–H bonds of the aryl rings,[31] remains approximately unchanged when [3]Ph$^+$ is oxidised to [3]Ph$^+$ in the CF–ACN, while the same signal broadens and weakens in CF–NM, following the same trend observed for the fingerprint Raman peak of neutral [3]Ph (2030 cm^{-1}). The remaining Raman signals below 1450 cm^{-1} can be assigned to vibrational features of the respective solvents.

To support the chemical oxidation of [3]Ph to [3]Ph$^+$, we explored electrochemical methods. Cyclic voltammetry (CV) was performed with [3]Ph dissolved in dichloromethane (DCM) at a concentration of 0.56 mmol L^{-1} (*ca.* 0.20 g L^{-1}), tetrabutylammonium tetrafluoroborate [(TBA)(TFB)] as a supporting electrolyte (0.1 mol L^{-1}), Pt gauze as the working electrode, and ferrocene as a reference (2 mmol L^{-1}); all potentials are reported *vs.* the Fc/Fc$^+$ couple, unless otherwise stated. The voltammogram of [3]Ph (Fig. 2(a)) shows a redox pair centered at +0.11 V, related to the oxidation of ferrocene (Fc/Fc$^+$), and another pair with $E_{1/2}$ at +0.80 V assigned to reversible oxidation [3]Ph, as this signal does not appear in the absence of [3]Ph (Fig. S5). Above +1.2 V, DCM starts to degrade and generates the observed current increase. $FeCl_3$ in ACN has a reduction potential of about +2.0 V *vs.* SCE (saturated calomel electrode),[57–59] which is *ca.* +1.6 V *vs.* Fc/Fc$^+$. Thus, the reduction potential of $FeCl_3$ is clearly sufficient to oxidise [3]Ph in weakly coordinating organic liquids, such as ACN or NM.

Chronoamperometry was then performed by fixing the electrical potential at +1.05 V for 300 s. The solution of [3]Ph near the working electrode (Pt) gradually turns from yellow to blue, which can be related to the oxidation of both [3]Ph and ferrocene. A solid precipitate appears after applying the voltage for a prolonged time (> *ca.* 3 min). This indicates the low solubility of the blue reaction product in DCM. The precipitating product is consistent with the formation of [3]Ph$^+$, a charged product that has limited solubility in weakly polar solvents, such as DCM. Raman spectra were collected by focusing the laser onto the Pt electrode, before and during the chronoamperometry, to compare the spectra acquired from the chemical and electrochemical oxidation (Fig. 2(b)). The spectrum collected from electrochemical oxidation presents two peaks in the sp-carbon stretching frequency region, at 2032 cm^{-1} related to [3]Ph, and the other at 2108 cm^{-1} as previously assigned to [3]Ph$^+$ in the chemical oxidation in solutions of CF–ACN and CF–NM (Fig. 1(d)). As observed in the case of chemical oxidation, the peak associated with the C=C stretching mode of [3]Ph (1596 cm^{-1}) is redshifted in [3]Ph$^+$ (1582 cm^{-1}), corroborating the change in the electronic structure upon formation of [3]Ph$^+$. The absence of the peak at 1613 cm^{-1} from the chronoamperometry experiment confirms its origin from a $FeCl_3$-mediated coordination complex during chemical oxidation, since $FeCl_3$ was not introduced in the former. The comparison between the two Raman spectra collected during the electrochemical and chemical oxidation experiments (middle and top curves in Fig. 2(b), respectively) confirm that [3]Ph$^+$ is formed in both cases. This assignment is corroborated by the corresponding UV-vis-NIR bands produced by [3]Ph$^+$ formed by chemical and electrochemical oxidation (Fig. 2(c)). The UV-vis-NIR absorption experiment during the electrochemical oxidation was carried out in the absence of ferrocene to avoid ambiguity between the two oxidation products, ferrocenium[60] and [3]Ph$^+$, since both absorb in the same wavelength range.

The successful oxidation of [3]Ph based on the regulation of concentration and solvent was the motivation to assess the extension of this strategy to sp^2-carbon-based molecular semiconductors with low lying HOMO energy levels. The heteroaromatic C8-BTBT (Fig. 3(a)) is a well-established, high-performing sp^2-based semiconductor. It has been widely employed in p-type OFETs both as a standalone active material and in

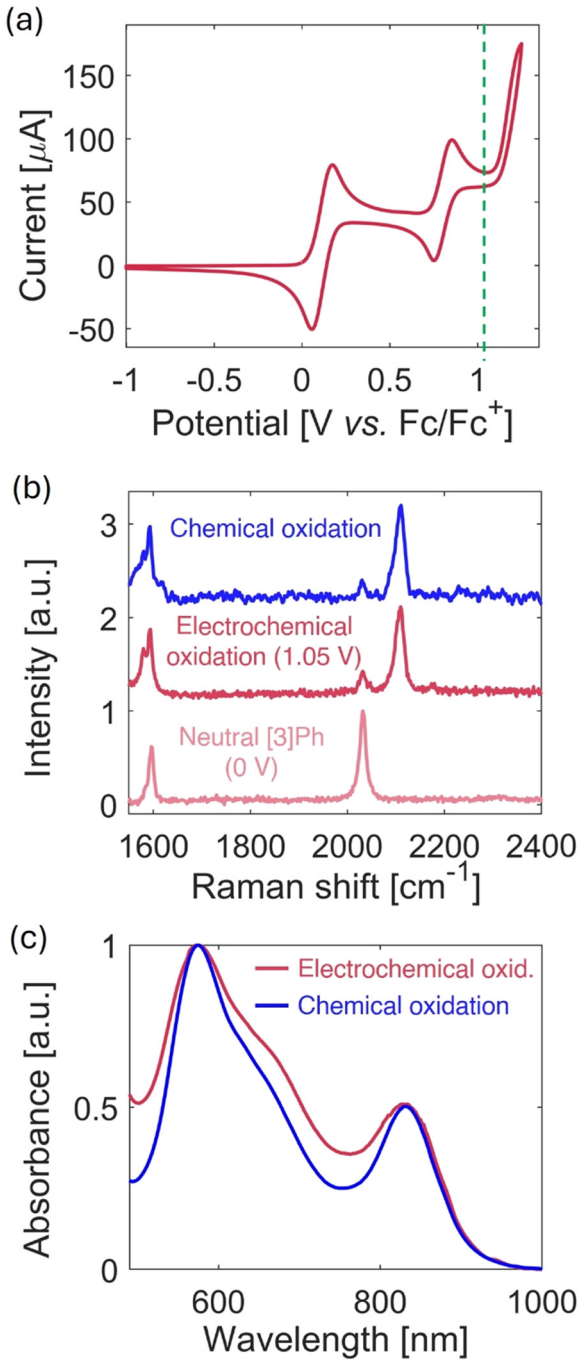

Fig. 2 (a) Cyclic voltammogram of [3]Ph (0.56 mmol L^{-1} in DCM) using ferrocene (FC) (2 mmol L^{-1}), as an internal reference, and [(TBA)(TFB)] (0.1 mol L^{-1}) as supporting electrolyte. Analyses were conducted between −1.0 and +1.25 V (50 mV s^{-1}), subsequently fixing the potential at 1.05 V for the chronoamperometry. (b) Raman spectra of a [3]Ph (1.8 mmol L^{-1}) solution in DCM acquired before electrochemical oxidation (neutral [3]Ph, pink curve at the bottom) and during a chronoamperometry experiment with fixed potential at +1.05 V for 300 s (red curve in the middle). The blue line shows the Raman spectrum acquired on a solution of [3]Ph:$FeCl_3$ (0.25 g L^{-1}/0.75 g L^{-1}) in CF–NM. (c) Comparison of UV-vis-NIR spectra, with normalised absorbances, of chemically oxidised [3]Ph (with $FeCl_3$, 0.25 g L^{-1}/0.75 g L^{-1} in CF–NM), and electrochemically oxidised [3]Ph (1.0 g L^{-1} in DCM without ferrocene, with [(TBA)(TFB)] 0.25 mol L^{-1} and after applying +1.1 V for about 15 s).

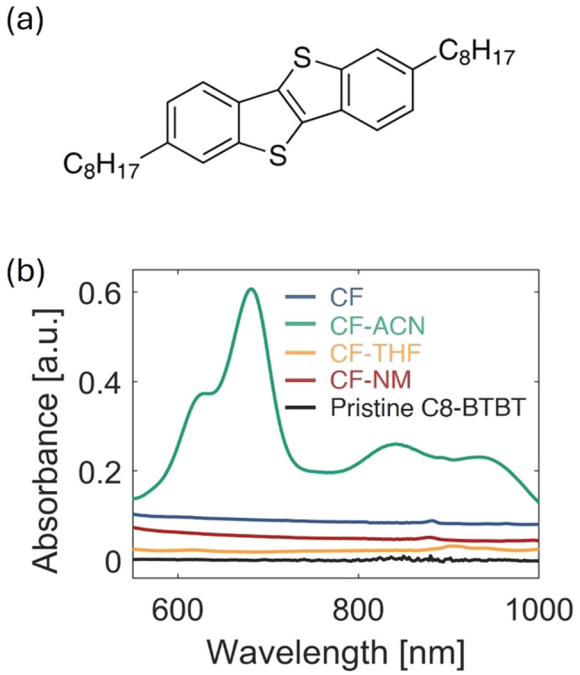

Fig. 3 (a) Molecular structure of C8-BTBT. (b) UV-Vis-NIR spectra, with a focus on the visible range, of C8-BTBT (final concentration: 0.13 g L^{-1}) mixed with $FeCl_3$ (5.4 g L^{-1}) in CF or solvent mixtures 1 : 1 by volume. The solvents added to CF are ACN, THF, and NM. In black, the spectrum of a diluted solution of C8-BTBT (0.052 g L^{-1}) in CF. All spectra were acquired with 4 mm quartz cuvettes.

combination with polymers, reaching field effect mobilities in excess 20 cm^2 V^{-1} s^{-1}.[61–65] The UV-vis-NIR spectra of solutions of C8-BTBT and $FeCl_3$ in the same solvent combinations used for [3]Ph (CF–ACN, CF–THF, CF–NM) are presented in Fig. 3(b). While all samples present strong absorptions in the UV region (Fig. S6 and Fig. 1(b)), only the mixture of C8-BTBT and $FeCl_3$ in CF–ACN can absorb in the visible region of the spectrum. The absorption band in this mixture has the same profile as reported for doped C8-BTBT.[66] The spectrum (Fig. 3(b)) thus suggests that C8-BTBT is oxidised by $FeCl_3$ in the solvent mixture CF–ACN. It is interesting to note that, unlike [3]Ph, C8-BTBT is not oxidised in the solvent mixture of CF–NM, confirming that the conditions necessary to force chemical oxidation of molecules with a deep HOMO necessitate tuning of the polar aprotic solvent mixture.

The reduction potential of $FeCl_3$ in organic media is affected by the solvent in terms of solvation, as expected for any compound,[67] but also by the possible presence of solid particles of $FeCl_3$ due to the incomplete dissolution. In fact, it is known that solid particles of $FeCl_3$ offer vacant sites on the surface of Fe(III) that can effectively initiate the oxidation process.[38] In contrast, in good solvents $FeCl_3$ tends to form dimers and/or coordination compounds with solvent molecules, which has the effect of passivating the vacant site of Fe(III).[68] The presence of solid $FeCl_3$ particles in the solvents has been assessed by the Tyndall effect.[69] Fig. S7 presents pictures of solutions of $FeCl_3$ (0.75 g L^{-1}) in CF, CF–ACN, CF–NM and CF–THF irradiated with a green laser. Light scattering from

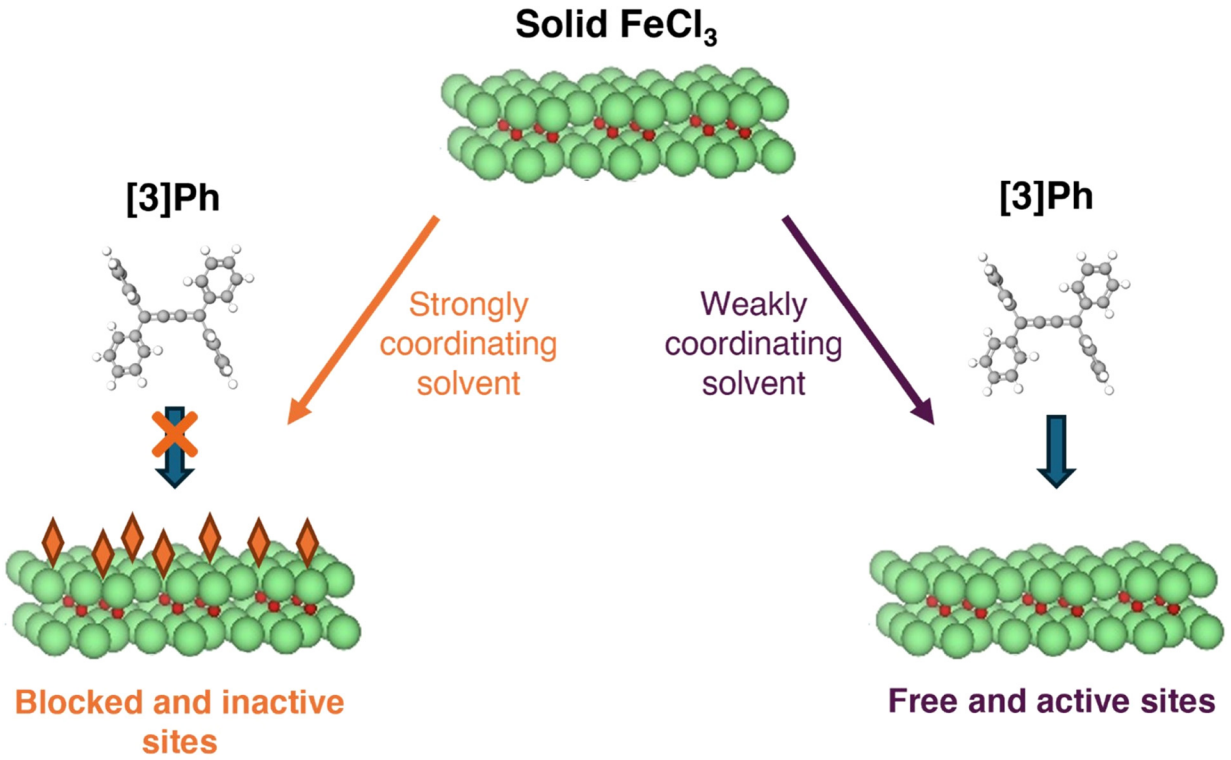

Fig. 4 Schematic representation of solid $FeCl_3$ (centre) and two possible mixtures in different liquid media: containing strongly coordinating solvents (orange diamonds), with blocked and inactive sites (left), or weakly coordinating solvents, with free and active sites towards oxidation (right).

particles is more evident in the system containing only CF and mixtures CF–ACN and CF–NM. While the Tyndall effect confirms that all systems contain dispersed solid particles, the mixture with CF–THF presents the weakest scattering, confirming a lower concentration and/or smaller size of dispersed $FeCl_3$ particles. Indeed, $FeCl_3$ was reported as soluble in diethyl ether,[38] which has acid–base behavior similar to THF and acts as a hard Lewis base.[47] Thus, the hard acid $FeCl_3$ is probably more soluble in THF than in the other liquids tested, which explains the lower number of solid particles and the corresponding weaker light scattering. Concerning the formation of lyophilic-like systems, this process can occur in the mixture containing THF, because it is a highly coordinating solvent and interacts strongly with iron(III) due to their common Lewis acid–base behavior.

The solubility and colloidal behavior of $FeCl_3$ in different solvents were further evaluated to understand its role as an oxidant. DLS measurements (Fig. S8) confirmed the presence of solid particles in all mixtures, with larger particle sizes in NM and more signal variation in THF, which is consistent with different degrees of dissolution. UV-vis and Raman spectroscopy (Fig. S9) showed that ACN and NM preserve $FeCl_3$ oxidative activity, while THF suppresses it. The results of homocoagulation experiments, shown in Fig. S10, demonstrated that $FeCl_3$ behaves as a lyophobic colloid in CF–ACN, stabilised by electrostatic interactions rather than solvation. Overall, weakly coordinating solvents (ACN and NM) favor more reactive colloidal dispersions, while strongly coordinating solvents (THF) passivate $FeCl_3$ surfaces and suppress oxidation (Fig. 4). These findings confirmed that the solvent choice is affecting not only the thermodynamic and kinetics of the oxidation process *via* solvation interactions between substrate and solvent molecules, but also the colloidal nature and the oxidative strength of $FeCl_3$.

Conclusions

In this work, an effective strategy for the oxidation of a cumulenic (sp-carbon) and heteroaromatic (sp^2-carbon) semiconductors with deep HOMO energy levels is achieved by leveraging the oxidative strength of $FeCl_3$ through optimisation of the solvent systems. This approach readily enables the oxidation of the model cumulene tetraphenylbutatriene, [3]Ph. A positive charge was successfully induced on [3]Ph through mixing with $FeCl_3$ in solution under optimised solvent conditions. The appearance of new UV-vis-NIR absorption bands in the visible region and a new Raman active mode (ECC) near 2100 cm^{-1} confirmed the formation of oxidised species, $[3]Ph^+$ (*i.e.*, the radical-cation). The observed blue-shift of the ECC mode upon oxidation is consistent with increased BLA and a more pronounced polyynic character of the cumulenic chain in the charged state. Electrochemical measurements combined with *in operando* Raman further validated these findings. The oxidation of [3]Ph by the $FeCl_3$ process is clearly related to the use of a mixture of chloroform with polar,

aprotic solvents, namely acetonitrile and nitromethane. The enhanced oxidation efficiency observed in optimised mixtures suggests that favorable intermolecular interactions of $FeCl_3$ with weakly coordinating solvents increase reactivity and stabilise the oxidised products. This approach to oxidation was successfully extended to the well-known heteroaromatic semiconductor C8-BTBT.

On the one hand, the successful oxidation of both [3]Ph and C8-BTBT (constructed from sp- and sp^2-hybridised carbon, respectively) demonstrates a versatile strategy to access the oxidised state of conjugated materials with deep HOMO energy levels with enhanced environmental stability. On the other hand, by identifying the charged state of [3]Ph, this work contributes to the fundamental understanding of cumulenes and offers ground for their effective exploitation in optoelectronic applications.

Author contributions

Elda Sala: data curation (lead), formal analysis (lead), investigation (lead), methodology (equal), validation (equal), writing – original draft (lead), and writing – review & editing (equal). João Paulo V. Damasceno: conceptualisation (equal), investigation (equal), methodology (equal), writing – original draft (lead), validation (supporting), and writing – review & editing (equal). Stefano Pecorario: conceptualisation (supporting), formal analysis (supporting), investigation (supporting), validation (equal), writing – review & editing (equal). Pietro Marabotti: formal analysis (supporting), investigation (supporting), and writing – review & editing (equal). Ivan K. Ilic: formal analysis (supporting), investigation (supporting), validation (equal), and writing – review & editing (equal). Valerio Galli: investigation (supporting) and writing – review & editing (equal). Simone Melesi: investigation (supporting), validation (equal), and writing – review & editing (equal). Pierfrancesco Sansò: investigation (equal), and writing – review & editing (equal). Andrea Tuarivoli: investigation (supporting) and writing – review & editing (equal). Carlo S. Casari: formal analysis (supporting), methodology (equal), supervision (equal), validation (equal), and writing – review & editing (equal). Daniele Fazzi: formal analysis (supporting), methodology (supporting), supervision (supporting), and writing – review & editing (equal). Rik R. Tykwinski: resources (equal), supervision (equal), validation (supporting), and writing – review & editing (equal). Mario Caironi: conceptualisation (equal), funding acquisition (lead), investigation (supporting), methodology (equal), project administration (lead), resources (equal), supervision (lead), validation (equal), writing – original draft (supporting), and writing – review & editing (equal).

Conflicts of interest

There are no conflicts to declare.

Data availability

Data supporting the findings of this study are available on IIT Dataverse at https://doi.org/10.48557/O51KSC. Such data will be made openly available on IIT Dataverse by the end of March 2026.

Supplementary information (SI): experimental methods, and supporting characterisation data. See DOI: https://doi.org/10.1039/d5ma01506e.

Acknowledgements

We thank Dr Bozheng Sun for the synthesis of [3]Ph, and Dr Pietro Rossi for his valuable suggestions throughout the experiments. D. F. acknowledges the projects funded by the National Recovery and Resilience Plan (NRRP), Mission 04 Component 2 Investment 1.5 – NextGenerationEU, Call for tender no. 3277 dated 30/12/2021, Award Number: 0001052 dated 23/06/2022, and the National Project funded by the European Union – Next Generation EU, Project title "Modelling and design of organic conjugated redox materials for energy-saving applications: a bottom-up strategy", code MUR 2022WKTH9E – CUP J53D23008810006. R. R. T. acknowledges funding from the Natural Sciences and Engineering Research Council of Canada (NSERC RGPIN-2017-05052 and RGPIN-2023-04000) and the Canada Foundation for Innovation (CFI). C. S. C. acknowledges partial funding from the European Research Council (ERC) under the European Union's Horizon 2020 Research and Innovation Program ERC Consolidator Grant (ERC CoG2016 EspLORE Grant Agreement 724610, website: https://www.esplore.polimi.it). C. S. C. also acknowledges funding from the project funded under the National Recovery and Resilience Plan (NRRP), Mission 4 Component 2 Investment 1.3 Call for Tender 1561 of 11.10.2022 of Ministero dell'Università e della Ricerca (MUR), funded by the European Union NextGenerationEU Award Project Code PE0000021, Concession Decree 1561 of 11.10.2022 adopted by Ministero dell'Università e della Ricerca (MUR), CUP D43C22003090001, Project "Network 4 Energy Sustainable Transition (NEST)". J. P. V. D. acknowledges The São Paulo State Research Foundation (FAPESP) for the postdoctoral fellowships (Processes: 2020/06604-9 and 2022/05053-4).

References

1 H. Sirringhaus, *Adv. Mater.*, 2014, **26**(9), 1319–1335.
2 C. Wang, H. Dong, L. Jiang and W. Hu, *Chem. Soc. Rev.*, 2018, **47**(2), 422–500.
3 S. Pecorario, A. D. Scaccabarozzi, D. Fazzi, E. Gutiérrez-Fernández, V. Vurro, L. Maserati, M. Jiang, T. Losi, B. Sun, R. R. Tykwinski, C. S. Casari and M. Caironi, *Adv. Mater.*, 2022, **34**(15), 2110468.
4 C. S. Casari, M. Tommasini, R. R. Tykwinski and A. Milani, *Nanoscale*, 2016, **8**, 4414–4435.
5 J. A. Januszewski and R. R. Tykwinski, *Chem. Soc. Rev.*, 2014, **43**(9), 3184–3203.
6 W. Luo and W. Windl, *Carbon*, 2009, **47**, 367–383.

7 D. Wendinger and R. R. Tykwinski, *Acc. Chem. Res.*, 2017, **50**(6), 1468–1479.
8 S. N. Spisak, M. U. Bühringer, Z. Wei, Z. Zhou, R. R. Tykwinski and M. A. Petrukhina, *Angew. Chem.*, 2019, **131**(7), 2045–2050.
9 M. Tommasini, A. Milani, D. Fazzi, A. Lucotti, C. Castiglioni, J. A. Januszewski, D. Wendinger and R. R. Tykwinski, *J. Phys. Chem. C*, 2014, **118**(45), 26415–26425.
10 C. S. Casari and A. Milani, *MRS Commun.*, 2018, **8**(2), 207–219.
11 W. A. Chalifoux and R. R. Tykwinski, *Nat. Chem.*, 2010, **2**(11), 967–971.
12 R. R. Tykwinski, W. Chalifoux, S. Eisler, A. Lucotti, M. Tommasini, D. Fazzi, M. Del Zoppo and G. Zerbi, *Pure Appl. Chem.*, 2010, **82**, 891–904.
13 M. Liu, V. I. Artyukhov, H. Lee, F. Xu and B. I. Yakobson, *ACS Nano*, 2013, **7**(11), 10075–10082.
14 M. Wang and S. Lin, *Sci. Rep.*, 2015, **5**, 18122.
15 N. D. Lang and P. Avouris, *Phys. Rev. Lett.*, 2000, **84**(2), 358–361.
16 S. Tongay, R. T. Senger, S. Dag and S. Ciraci, *Phys. Rev. Lett.*, 2004, **93**, 136404.
17 N. D. Lang and P. Avouris, *Phys. Rev. Lett.*, 1998, **81**(16), 3515.
18 A. Milani, M. Tommasini, M. Del Zoppo, C. Castiglioni and G. Zerbi, *Phys. Rev. B: Condens. Matter Mater. Phys.*, 2006, **74**, 15.
19 A. Milani, M. Tommasini and G. Zerbi, *J. Chem. Phys.*, 2008, **128**, 6.
20 M. Tommasini, A. Milani, D. Fazzi, M. Del Zoppo, C. Castiglioni and G. Zerbi, *Phys. E*, 2008, **40**(7), 2570–2576.
21 S. Gunasekaran and L. Venkataraman, *J. Chem. Phys.*, 2020, **153**(12), 124304.
22 A. G. Whittaker, P. P. K. Smith and P. R. Buseck, *Science*, 1985, **229**(4712), 485–487.
23 A. Milani, M. Tommasini, V. Russo, A. L. Bassi, A. Lucotti, F. Cataldo and C. S. Casari, *Beilstein J. Nanotechnol.*, 2015, **6**(1), 480–491.
24 J. A. Januszewski, D. Wendinger, C. D. Methfessel, F. Hampel and R. R. Tykwinski, *Angew. Chem.*, 2013, **52**(6), 1817.
25 S. Melesi, P. Marabotti, A. Milani, B. Pigulski, N. Gulia, P. Pińkowski, S. Szafert, M. Del Zoppo, C. Castiglioni and C. S. Casari, *J. Phys. Chem. A*, 2024, **128**(14), 2703–2716.
26 C. Wang, A. S. Batsanov, M. R. Bryce, S. Martín, R. J. Nichols, S. J. Higgins, V. M. García-Suárez and C. J. Lambert, *J. Am. Chem. Soc.*, 2009, **131**(43), 15647–15654.
27 P. Moreno-García, M. Gulcur, D. Z. Manrique, T. Pope, W. Hong, V. Kaliginedi, C. Huang, A. S. Batsanov, M. R. Bryce, C. Lambert and T. Wandlowski, *J. Am. Chem. Soc.*, 2013, **135**(33), 12228–12240.
28 M. Gulcur, P. Moreno-García, X. Zhao, M. Baghernejad, A. S. Batsanov, W. Hong, M. R. Bryce and T. Wandlowski, *Chem. – Eur. J.*, 2014, **20**(16), 4653–4660.
29 X. Wu, L. Wang, Y. Hua, C. Wang, A. S. Batsanov and M. R. Bryce, *Tetrahedron*, 2014, **70**(11), 2015–2019.
30 S. Ghosh, M. Righi, S. Melesi, Y. Qiu, R. R. Tykwinski and C. S. Casari, *Carbon*, 2025, **234**, 119952.
31 A. D. Scaccabarozzi, A. Milani, S. Peggiani, S. Pecorario, B. Sun, R. R. Tykwinski, M. Caironi and C. S. Casari, *J. Phys. Chem. Lett.*, 2020, **11**(5), 1970–1974.
32 H. Bronstein, C. B. Nielsen, B. C. Schroeder and I. McCulloch, *Nat. Rev. Chem.*, 2020, **4**(2), 66–77.
33 A. D. Scaccabarozzi, A. Basu, F. Aniés, J. Liu, O. Zapata-Arteaga, R. Warren, Y. Firdaus, M. I. Nugraha, Y. Lin, M. Campoy-Quiles, N. Koch, C. Müller, L. Tsetseris, M. Heeney and T. D. Anthopoulos, *Chem. Rev.*, 2022, **122**(4), 4420–4492.
34 X. Qiao, X. Wang and Z. Mo, *Synth. Met.*, 2001, **122**(2), 449–454.
35 D. D. Diaz, P. O. Miranda, J. I. Padron and V. S. Martin, *Curr. Org. Chem.*, 2006, **10**(4), 457–476.
36 A. A. O. Sarhan and C. Bolm, *Chem. Soc. Rev.*, 2009, **38**(9), 2730–2744.
37 R. D. McCullough, *Adv. Mater.*, 1999, **10**(2), 93.
38 V. M. Niemi, P. Knuuttila, J. E. Osterholm and J. Korvola, *Polym.*, 1992, **33**(7), 1559–1562.
39 Y. Liu, N. Nishiwaki, K. Saigo and R. Sugimoto, *Bull. Chem. Soc. Jpn.*, 2013, **86**(9), 1076–1078.
40 T. Olinga and B. François, *Synth. Met.*, 1995, **69**(1–3), 297–298.
41 X. Qiao, X. Wang and Z. Mo, *Synth. Met.*, 2001, **122**(2), 449–454.
42 T. A. P. Hai and R. Sugimoto, *Polym. J.*, 2016, **48**(12), 1115–1121.
43 Y. Liu, N. Nishiwaki, K. Saigo and R. Sugimoto, *Polym. Bull.*, 2015, **72**(7), 1817–1826.
44 P. E. Hoggard, M. Gruber and A. Vogler, *Inorg. Chim. Acta*, 2003, **346**, 137–142.
45 R. G. Pearson, *J. Chem. Educ.*, 1968, **45**(9), 581.
46 R. G. Pearson, *J. Chem. Educ.*, 1968, **45**(10), 643.
47 W. B. Jensen, *Chem. Rev.*, 1978, **78**(1), 1–22.
48 J. E. Huheey, E. A. Keiter and K. Harper, *Inorganic Chemistry: Principles of Structure and Reactivity*, Harper Collins, New York, 4th edn, 1993.
49 A. D. Laurent and D. Jacquemin, *Int. J. Quantum Chem.*, 2013, **113**(17), 2019–2039.
50 S. Sebastian, V. Riley, B. Wanniarachchi, C. Ritchie and L. Goerigk, *RSC Adv.*, 2025, **15**(28), 22419–22431.
51 N. R. Agarwal, A. Lucotti, D. Fazzi, M. Tommasini, C. Castiglioni, W. A. Chalifoux and R. R. Tykwinski, *J. Raman Spectrosc.*, 2013, **44**, 1398–1410.
52 A. Milani, M. Tommasini, D. Fazzi, C. Castiglioni, M. Del Zoppo and G. Zerbi, *J. Raman Spectrosc.*, 2008, **39**, 164–168.
53 A. Lucotti, M. Tommasini, D. Fazzi, M. Del Zoppo, W. A. Chalifoux, M. J. Ferguson, G. Zerbi and R. R. Tykwinski, *J. Am. Chem. Soc.*, 2009, **131**(12), 4239–4244.
54 A. Milani, A. Lucotti, V. Russo, M. Tommasini, F. Cataldo, A. Li Bassi and C. S. Casari, *J. Phys. Chem. C*, 2011, **115**, 12836–12843.
55 N. R. Agarwal, A. Lucotti, D. Fazzi, M. Tommasini, C. Castiglioni, W. A. Chalifoux and R. R. Tykwinski, *J. Raman Spectrosc.*, 2013, **44**(10), 1398–1410.
56 S. N. Spisak, M. U. Bühringer, Z. Wei, Z. Zhou, R. R. Tykwinski and M. A. Petrukhina, *Angew. Chem.*, 2019, **131**(7), 2045–2050.
57 I. E. Jacobs, Y. Lin, Y. Huang, X. Ren, D. Simatos, C. Chen, D. Tjhe, M. Statz, L. Lai, P. A. Finn, W. G. Neal, G. D'Avino,

V. Lemaur, S. Fratini, D. Beljonne, J. Strzalka, C. B. Nielsen, S. Barlow, S. R. Marder, I. McCulloch and H. Sirringhaus, *Adv. Mater.*, 2022, **34**(22), 2102988.
58 Y. Wei, C. C. Chan, J. Tian, G. W. Jang and K. F. Hsueh, *Chem. Mater.*, 1991, **3**(5), 888–897.
59 A. F. Diaz, J. Crowley, J. Bargon, G. P. Gardini and J. B. Torrance, *J. Electroanal. Chem. Interfacial Electrochem.*, 1981, **121**, 355–361.
60 C. Swearingen, J. Wu, J. Stucki and A. Fitch, *Environ. Sci. Technol.*, 2004, **21**(38), 5598–5603.
61 P. Xie, T. Liu, J. Sun and J. Yang, *Adv. Funct. Mater.*, 2022, **32**, 21.
62 Z. Zhang, B. Peng, X. Ji, K. Pei and P. K. L. Chan, *Adv. Funct. Mater.*, 2017, **27**, 37.
63 D. Zhang, X. Zheng, C. He, Y. He and H. Meng, *Appl. Phys. Lett.*, 2024, **124**, 12.
64 A. Basu, M. R. Niazi, A. D. Scaccabarozzi, H. Faber, Z. Fei, D. H. Anjum, A. F. Paterson, O. Boltalina, M. Heeney and T. D. Anthopoulos, *J. Mater. Chem. C*, 2020, **8**(43), 15368–15376.
65 T. Losi, F. A. Viola, E. Sala, M. Heeney, Q. He, H. Kleemann and M. Caironi, *Small Methods*, 2024, **8**(12), 2400546.
66 A. Babuji, A. Cazorla, D. Solano, C. Habenicht, H. Kleemann, C. Ocal, K. Leo and S. Barrena, *ACS Appl. Mater. Interfaces*, 2022, **14**, 44632–44641.
67 H. Svith, H. Jensen, J. Almstedt, P. Andersson, T. Lundbäck, K. Daasbjerg and M. Jonsson, *J. Phys. Chem. A*, 2004, **108**, 4805–4811.
68 S. A. Cotton, *J. Coord. Chem.*, 2018, **71**(21), 3415–3443.
69 W. B. Russel, D. A. Saville and W. R. Schowalter, *Colloidal Dispersions*, Cambridge University Press, 1991.